Supplementary Materials

SUPPLEMENTAL MATERIALS

Supplemental Figures

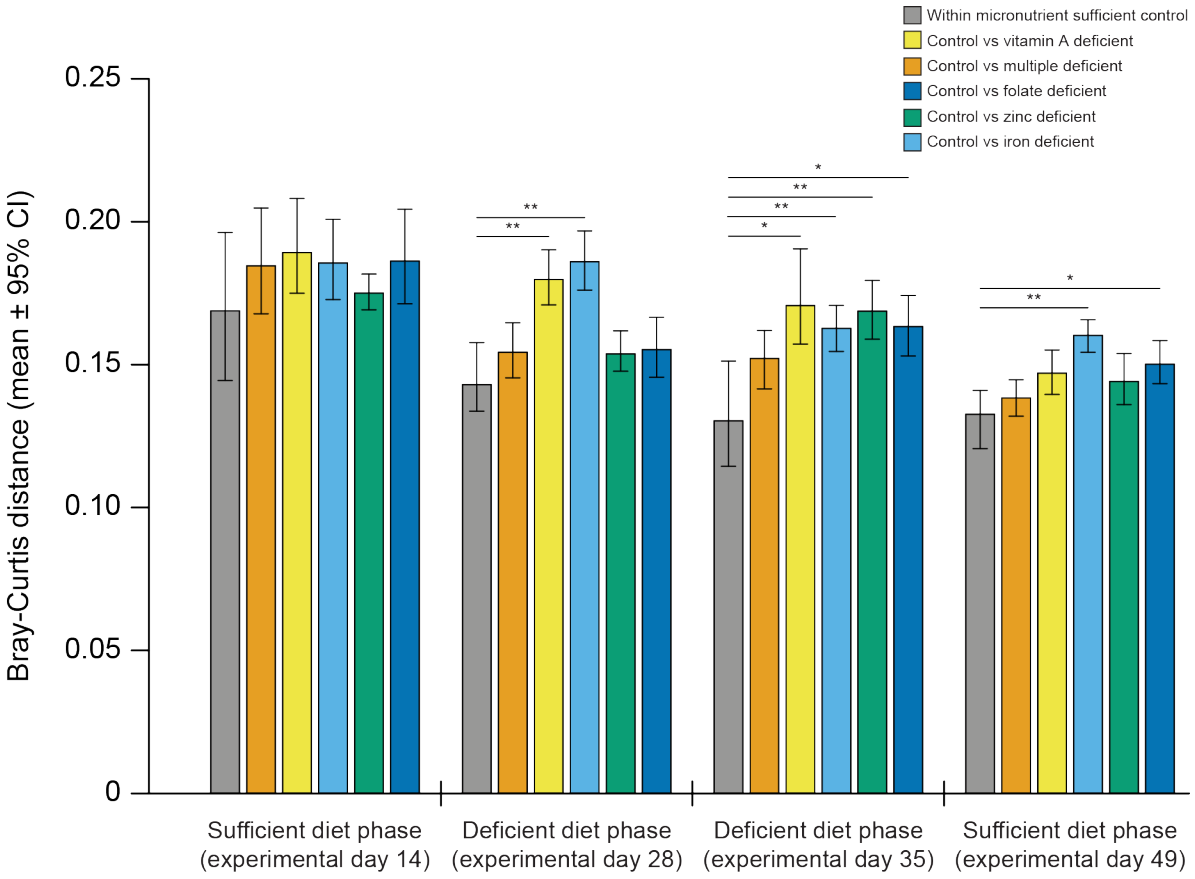

Fig. S1. Comparisons of community structure across experimental stages. Mean Bray-Curtis dissimilarities between the control group monotonously fed the micronutrient sufficient diet and each experimental treatment group were compared to the mean within-group dissimilarities for the control group. Bias-corrected and accelerated confidence intervals were calculated using 10,000 bootstrap re-samplings, with replacement. The significance of each comparison was determined as the proportion of 10,000 randomizations that generated absolute differences in mean dissimilarities more extreme than the observed difference. *P*-values were FDR-corrected after setting the minimum value to 0.0001. *, $P<0.05$; **, $P<0.01$.

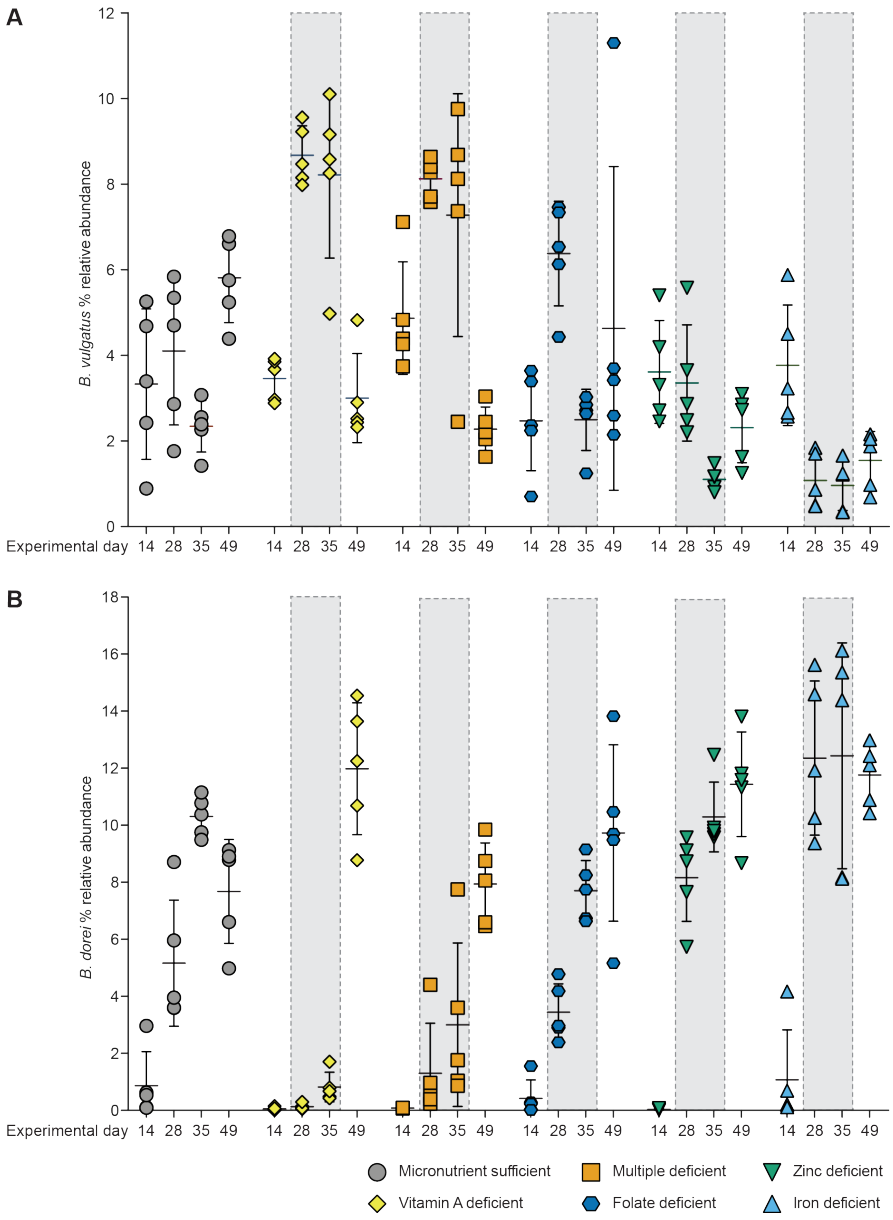

Fig. S2. Relative abundance of *B. vulgatus* ATCC 8482 and *B. dorei* DSM 17855 in gnotobiotic mice across experimental stages and treatment groups. COPRO-Seq analysis of the effects of the micronutrient-deficient versus sufficient diets on the relative abundances of (**A**) *B. vulgatus* and (**B**) *B. dorei*. Each data point indicates the relative abundance of the indicated organism in each mouse at the indicated experimental day and are coded by color to indicate experimental group. Grey-shaded boxes indicate time points for which mice were exposed to the specified micronutrient-deficient diet. Mean

values ± SD are indicated by bars. See table S4 and table S5 for the results of statistical tests of observed differences within and between treatment groups.

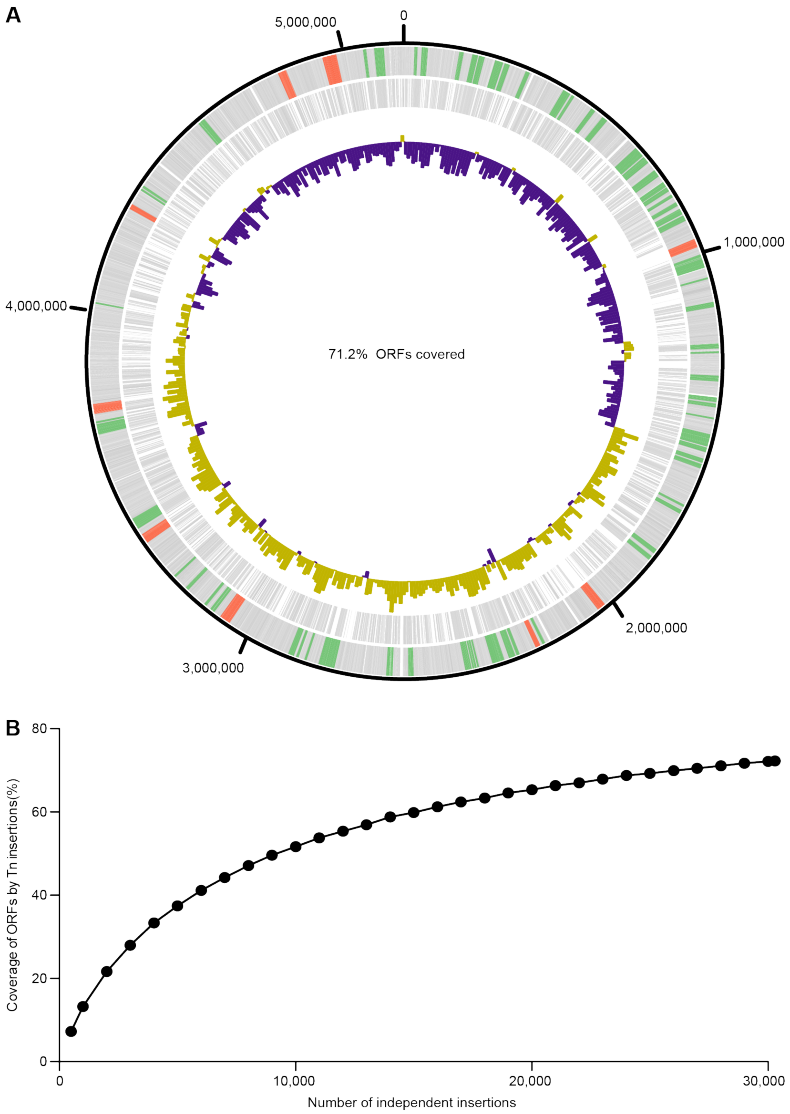

Fig. S3. Characterization of the *B. vulgatus* ATCC 8482 INSeq library. (**A**) Distribution of Tn mutants in the genome of *B. vulgatus* ATCC 8482. Key; Track 1 (innermost circle), plot of GC skew for the genome using a sliding window size of 10kb (yellow, GC skew > 0; purple, GC skew < 0); Track 2 (middle circle), genes with transposon insertions are depicted in light grey; Track 3 (outermost circle), all genes in the genome are shown with those represented in polysaccharide utilization loci (PULs) colored green, components of capsular polysaccharide synthesis (CPS) loci colored red, and all others colored light grey. (**B**) Estimating the saturation of *B. vulgatus* ATCC 8482 transposon mutant libraries by *in silico* simulation.

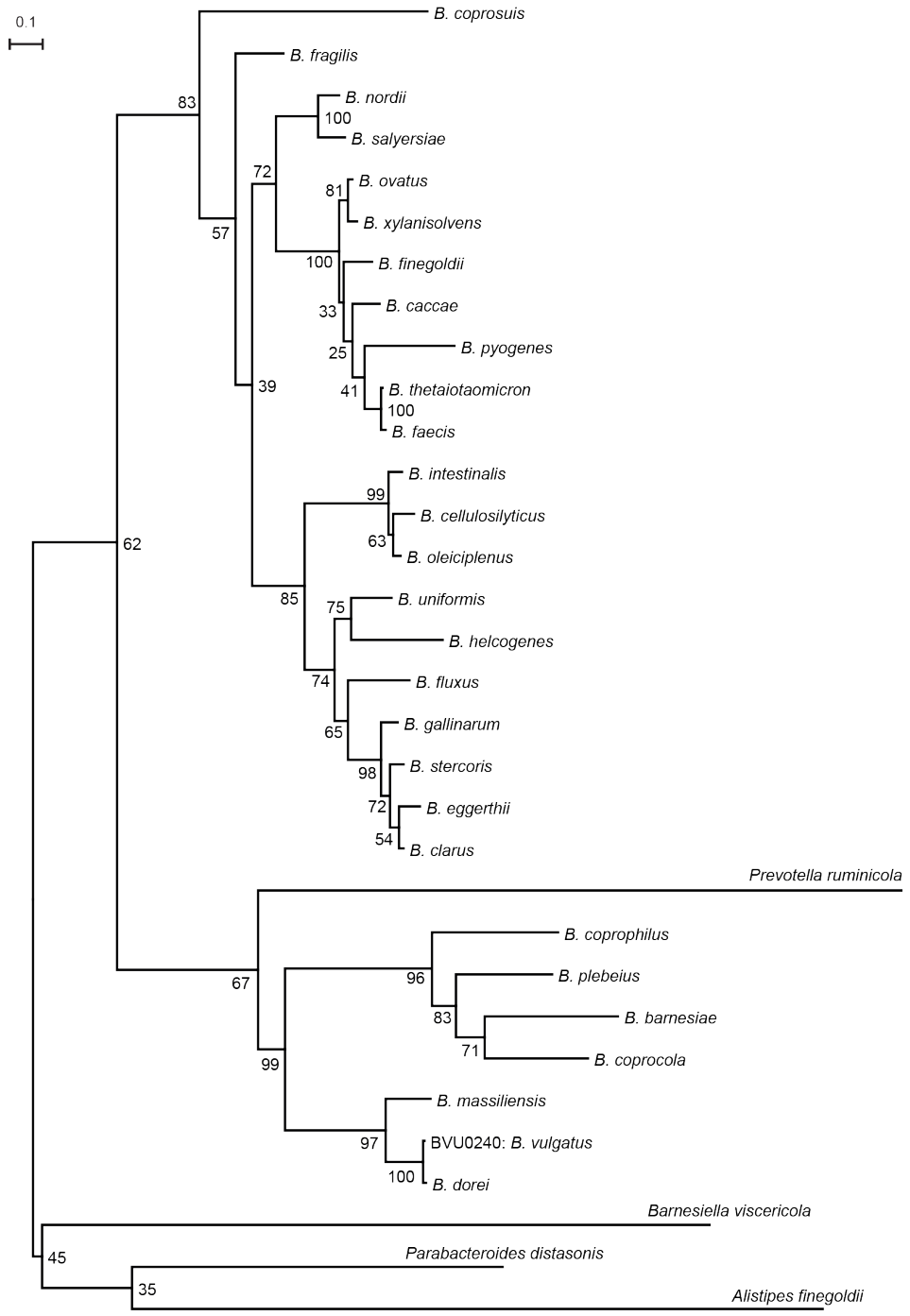

Fig. S4. Maximum likelihood phylogenetic tree of BVU0240/AcrR orthologs identified in human gut-associated *Bacteroides* and other members of the family Bacteroidaceae. Multiple amino acid sequence alignments were generated using ClustalX and exported in PHYLIP format. PhyML was used to generate the maximum likelihood tree, with bootstrap support (out of 100) indicated for given nodes.

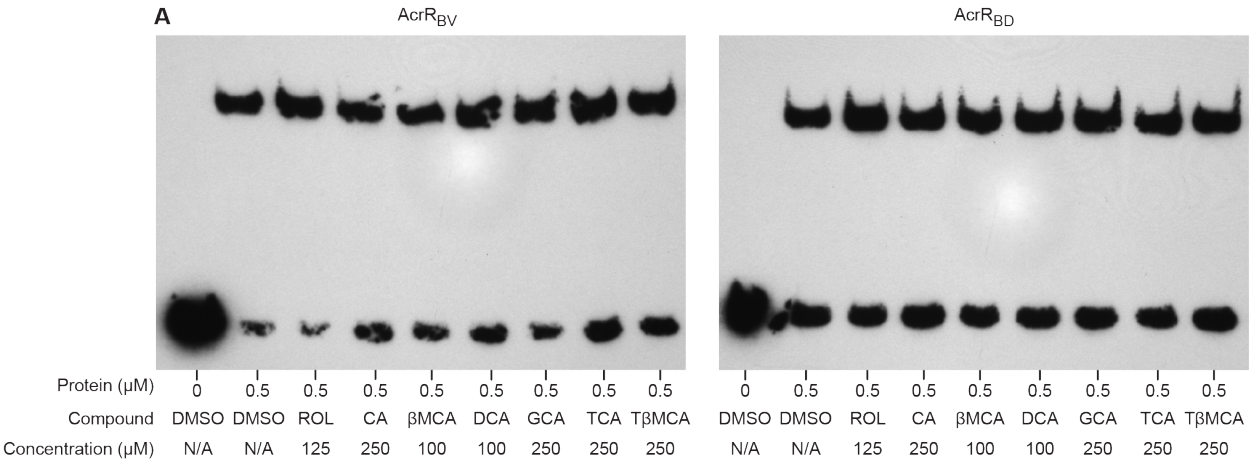

B

	K_d (FPA)	
Compound	**AcrR$_{BV}$**	**AcrR$_{BD}$**
DMSO (1%)	18.5 ± 6.2 nM	25.5 ± 10.9 nM
Retinol (125 μM)	49.5 ± 11.6 nM	56.5 ± 25.1 nM

C

	K_d (FPA)	
Compound	**AcrR$_{BV}$**	**AcrR$_{BD}$**
DMSO (1%)	9.4 ± 2.4 nM	19.3 ± 6.8 nM
CA (100 μM)	14.7 ± 3.5 nM	48.2 ± 14.5 nM
βMCA (100 μM)	12.3 ± 3.9 nM	53.5 ± 33.4 nM
DCA (100 μM)	20.2 ± 10.0 nM	74.0 ± 35.5 nM
GCA (100 μM)	23.9 ± 6.6 nM	51.0 ± 13.7 nM
TβMCA (100 μM)	65.2 ± 29.6 nM	28.2 ± 7.1 nM
TCA (100 μM)	12.5 ± 5.0 nM	45.2 ± 14.4 nM

Fig. S5. DNA-binding characteristics of AcrR$_{BV}$ and AcrR$_{BD}$ in the presence and absence of possible effectors. (**A**) Electrophoretic Mobility Shift Assays (EMSA) of AcrR$_{BV}$ and AcrR$_{BD}$ in the presence and absence of retinol and various bile acid species. (**B,C**) Binding characteristics (K_d) derived from curve fitting of Fluorescence Polarization (FP) Assay data for AcrR$_{BV}$ and AcrR$_{BD}$ in the presence and absence of (**B**) retinol or (**C**) bile acid species. FP data are reported as mean values ± SEM for experiments performed in triplicate. Abbreviations: ROL, retinol; CA, βMCA, β-muricholic acid; DCA, deoxycholic acid; GCA, glycocholic acid; TCA, taurocholic acid; TβMCA, tauro-β-muricholic acid.